Landscape and Urban Planning 136 (2015) 97–109

Contents lists available at ScienceDirect

Landscape and Urban Planning

journal homepage: www.elsevier.com/locate/landurbplan

Research paper

The impact of urban residential development patterns on forest carbon density: An integration of LiDAR, aerial photography and field mensuration

Christopher Godwin [a], Gang Chen [a,*], Kunwar K. Singh [b]

[a] Department of Geography and Earth Sciences, University of North Carolina at Charlotte, 9201 University City Blvd, Charlotte, NC 28223, USA
[b] Northern Plant Ecology Lab, Department of Biology, University of Saskatchewan, 112 Science Place, Saskatoon, SK, Canada S7N5E2

HIGHLIGHTS

- The impact of urban residential patterns on forest carbon density was explored.
- LiDAR and aerial photography were integrated for spatially explicit carbon mapping.
- Charlotte has a total amount of 3.8 million tonnes carbon ($298 million value).
- The impact of urban patterns varies across different densities of neighborhoods.

ARTICLE INFO

Article history:
Received 23 October 2014
Received in revised form 9 December 2014
Accepted 11 December 2014

Keywords:
Urban forest
Carbon density
Development pattern
LiDAR (light detection and ranging)
Aerial photography
Landscape metrics

ABSTRACT

Urban development continues to reshape forest landscapes and influence the carbon storage capacity of trees. To date, the impact of urban patterns on forest carbon density remains to be systematically evaluated. A major challenge is the lack of accurate and spatially explicit estimates of forest carbon storage over the entire urbanized area. In this study, we first developed an integrated approach that synergizes remote sensing LiDAR (light detection and ranging) and aerial photography to efficiently model landscape-level forest carbon storage in an urban environment at a fine resolution of 20 m. Using a case study in the Charlotte Metropolitan Region, USA, we were able to determine the total amount of carbon stored in the local forests to be 3.8 million tonnes ($298 million value), with an average carbon density of 53.6 t/ha. We further applied statistical analysis to investigate the relationship between urban developed patterns (i.e., landscape metrics) and forest carbon density in four types of residential neighborhoods (categorized by percent built-up ranging from low, medium-low, medium-high to high density). Results indicate a decrease of forest carbon density with an increase of carbon variance in neighborhoods where the intensity of development became higher. Residential neighborhoods with a higher built-up density were more likely to be affected by a larger number of landscape metrics. This indicates that a proper design of the neighborhood level urban spatial patterns (especially in high density neighborhoods) is essential to maximizing forest carbon storage at the landscape level.

Published by Elsevier B.V.

1. Introduction

Urban forests (i.e., trees in urban areas) are high quality carbon sinks to mitigate climate change by capturing carbon dioxide (CO_2) from the atmosphere. In the United States, trees growing on the urban land that accounts for 3% of the total landmass can sequester 14% of the amount of carbon sequestered by the entire nation's forests (Heath, Smith, Skog, Nowak, & Woodall, 2011). Nowak, Greenfield, Hoehn, and Lapoint (2013) estimated that the volume of carbon stored by urban forests in the United States is 643 million tonnes ($50.5 billion value) and their annual carbon sequestration is approximately 25.6 million tonnes ($2.0 billion value). With continued urban growth and sprawl, forests in these areas are expected to play a more critical role in climate change mitigation and associated initiatives, such as carbon offset trading (Poudyal, Siry, & Bowker, 2011; Strohbach & Haase, 2012).

Recent studies have demonstrated that the amount of carbon (per unit of tree cover) stored by urban forests is spatially non-stationary and highly related to regional context (Liu & Li, 2012;

* Corresponding author. Tel.: +1 704 687 5947; fax: +1 704 687 5966.
E-mail addresses: godwinschristopher@gmail.com (C. Godwin), gang.chen@uncc.edu (G. Chen), kun2001@gmail.com (K.K. Singh).

http://dx.doi.org/10.1016/j.landurbplan.2014.12.007
0169-2046/Published by Elsevier B.V.

McPherson, 1998; McPherson, Xiao, & Aguaron, 2013; Nowak et al., 2013; Strohbach and Haase, 2012; Zhao, Kong, Escobedo, & Gao, 2010). For example, during the mapping of urban forest carbon storage across the conterminous United States, McPherson et al. (2013) and Nowak et al. (2013) found large variations in the aggregated city-level estimates of carbon density, mainly attributed to the complex local and regional determinants (e.g., land development patterns) that influence tree species composition, stand density and forest growth. Within city boundaries, the differences in tree management practices, neighborhood age or land-use types further reveal high impacts on forest carbon storage across neighborhoods (Grove et al., 2006; Zhao et al., 2010). Despite these encouraging findings, few studies have systematically quantified the impacts of urban development patterns on forest carbon density at the inner-city neighborhood level (Ren et al., 2013). Landscape patterns are often quantified using landscape metrics, which refer to a broad range of quantitative indices representing spatial heterogeneity, such as characteristics of patches, classes of patches, or entire landscape mosaics (Herold, Scepan, & Clarke, 2002; McGarigal, Cushman, Neel, & Ene, 2002; Plexida, Sfougaris, Ispikoudis, & Papanastasis, 2014; Richardson & Moskal, 2011; Riitters et al., 1995; Seto & Fragkias, 2005; Wu, Shen, Sun, & Tueller, 2003). Judiciously analyzing the relationship between landscape metrics and forest carbon density informs the practices on efficient city tree management and sustainable urban environmental design (Termorshuizen & Opdam, 2009; Xiang, 2014).

To date, a major challenge confronting such analysis is the lack of accurate, up-to-date, and spatially explicit carbon estimates over the entire urban landscapes. For logistical and privacy reasons (up to 90% of urban trees are on private land in the U.S.), field observation using limited number of plots may cause large errors in sampling and leads to high uncertainties in carbon estimation (Clark, Matheny, Cross, & Wake, 1997; McPherson et al., 2013). Conventional optical remote sensing provides a viable alternative to study Earth surface of large geographical coverage in a timely and cost-effective manner. However, researchers have noticed that optical sensors are limited in their capabilities for capturing the understory vegetation in multi-strata forests, and the inaccurate retrieval of tree vertical structure makes carbon estimation a challenging task (Lu, 2005). Over the past decade, airborne LiDAR technology has attracted increased attention for measuring forest carbon density across biomes (Chen, Wulder, White, Hilker, & Coops, 2012). Lefsky et al. (2002) applied LiDAR to estimate aboveground biomass (ABG) of three species groups (temperate deciduous, temperate coniferous, and boreal coniferous biomes) using a single regression, which still explained 84% of variance in biomass. Asner et al. (2012) developed a universal LiDAR model for four tropical regions to estimate forest carbon density at a relatively high accuracy ($R^2 = 0.80$). In an effort to study urban forests of Oklahoma, Shrestha and Wynne (2012) evaluated the performance of LiDAR biomass modeling at the individual tree level. Despite a high diversity of tree growth rates and plant species types in local forests, their research unveiled a good agreement between LiDAR estimates and field measurements ($R^2 = 0.63$) making LiDAR a promising tool to offer high-accuracy and wall-to-wall forest carbon estimates over large urbanized areas (Seto, Güneralp, & Hutyra, 2012).

The primary goal of this research was to explore the impact of urban development patterns on forest carbon density at the neighborhood level. Here, we emphasize on the residential neighborhoods, because the majority of urban forests are located in these areas where trees also have high impacts on property values (Escobedo, Adams, & Timilsina, in press). To achieve the goal, we integrated LiDAR, aerial photography and field mensuration to extract spatially explicit forest carbon distribution and landscape metrics over the entire urbanizing landscapes of the study area.

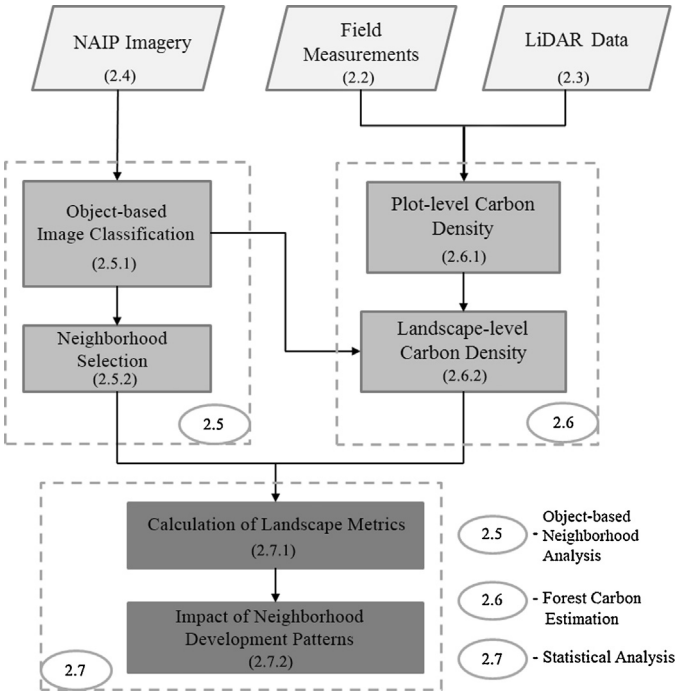

Fig. 1. Analytical schematics for the study with reference to Section 2.

Statistical analysis was then used to quantify the relationship between landscape metrics and carbon density. The flowchart in Fig. 1 summarizes these steps; while the following sections provide greater details and explanations.

2. Methods

2.1. Study area

The study area (1415 km^2 and centered at 35°15′N, 80°50′W) is located in Mecklenburg County of North Carolina, United States (Fig. 2). The region is often referred to as Charlotte–Mecklenburg County or the Charlotte Metropolitan Area. The rolling landscape of the region is characterized by the southern Piedmont physiography with secondary growth forests that have developed on former timber plantation sites and abandoned agricultural lands. Elevation of the County ranges from 252 m above sea level in the north to 159 m in the southern part. Forested landscapes, initially covered by widespread mixed oak forests interspersed with prairies, represent a mix of oak, hickory and pine. Mecklenburg County is one of the fastest developing regions of the southeastern United States. According to a report of U.S. Census Bureau (2013), it has grown in population from 0.4 million in 1980 to approximately 1 million people in 2013, a trend that is expected to continue. During the similar period between 1985 and 2008, the region lost 33% of its tree canopy and gained 60% developed land (Singh, Vogler, Shoemaker, & Meentemeyer, 2012). The rapid population growth, characterized by urban sprawl with low to high housing density, has replaced forest and farmland dominated landscapes with an array of developed land use types including managed treescapes and highly fragmented urban forests.

2.2. Field measurements

A total of 75 circular field plots (0.04 ha each) were measured during the years of 2010–2012 in vegetated areas covering all major forest types. The plots were designed following the typically used i-Tree ECO (Urban Forest Effects; also known as UFORE)

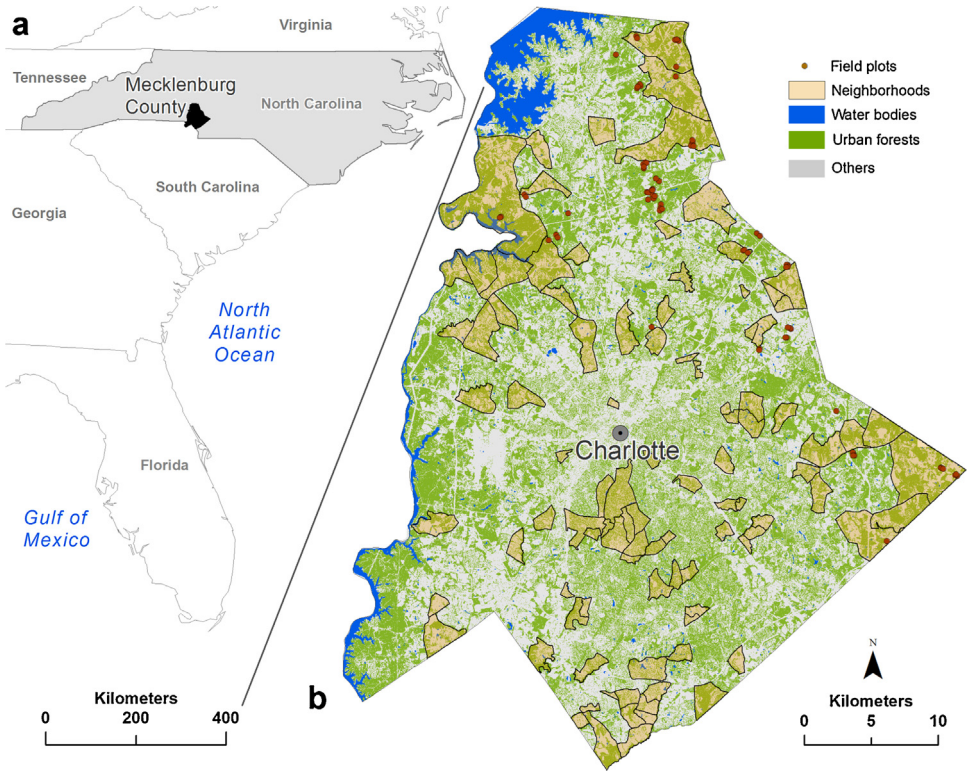

Fig. 2. (a) Study area is located in Mecklenburg County, North Carolina, USA. (b) Charlotte is the county seat and the largest city in North Carolina. (c) Selected neighborhoods are in orange polygons and the locations of field data are represented by circular plots.

protocols in urban forest studies (Nowak, Crane, Stevens, Hoehn, & Walton, 2008). Minor adjustments were performed on site selection under the consideration of site accessibility. Within each plot, tree diameter at the breast height (DBH), species composition, and merchantable tree height were recorded.

To acquire forest carbon density from field plots, we first applied Jenkins allometric equations (Jenkins, Chojnacky, Heath, & Birdsey, 2003) to calculate above-ground biomass (AGB) for each plot using tree species and DBH. Jenkins et al. (2003) complied (and modified some of the) 2640 equations based on a thorough review of published equations for U.S. species. The comparison of biomass estimates using Jenkins equations and the U.S. forest inventory data for eastern U.S. species suggested a general agreement (approximately ±30%; Jenkins et al., 2003). Despite the errors in calculating biomass, these equations were employed in this study because local equations were (and are still) not available and destructive sampling to accomplish such goal was not feasible. As further pointed out by McPherson et al. (2013), even if local AGB equations exist, they are often biased to public street and park trees, and forest biomass in open-grown conditions (e.g., street trees) tends to differ from that in closely-spaced areas (e.g., remnant large tree patches). Sampling errors, which are normally unknown, are another error source to increase uncertainty in forest biomass estimation (Nowak et al., 2013). To calculate the whole tree biomass, below-ground biomass (BGB) should be integrated with AGB. However, the knowledge of BGB in roots of urban is still limited (McPherson et al., 2013). Here, the AGB estimates were converted to full biomass by applying a root-to-shoot ratio of 0.26 (Cairns, Brown, Helmer, & Baumgardner, 1997). This ratio was used in our study based on the consideration of the relatively high model performance in root biomass estimation ($R^2 = 0.84$) conducted by Cairns et al. (1997), and its proved feasibility in several recent forest studies across U.S. cities (e.g., Nowak et al., 2008; Schmitt-Harsh, Mincey, Patterson, Fischer, & Evans, 2013). Finally, the biomass estimates were converted to carbon by multiplying the constant 0.5 (Lieth, 1975), which has been a standard factor for biomass-carbon conversion in both the natural and urban forest research (Hudak et al., 2012; McPherson et al., 2013; Myneni et al., 2001). Within each plot, the summarized tree-level carbon estimate was divided by 0.04 ha (size of plot) to obtain carbon density (t/ha).

We categorized all plots into the deciduous, coniferous and mixed types using a threshold of three-fourth that has been used in local forest management. Specifically, if a plot consists of over 75% deciduous or coniferous trees, it was labeled as a deciduous or coniferous plot; otherwise, it was labeled as a mixed plot. Four field plots were excluded from the subsequent analyses because of their unrealistic carbon estimates. Finally, a total of 71 plots (i.e., 25 deciduous, 21 coniferous, and 25 mixed) were selected; and their carbon density with descriptive statistics are summarized in Table 1.

2.3. LiDAR data

LiDAR data covering the entire study area were acquired from the Storm Water Services Division of Charlotte–Mecklenburg County government office in 1896 tiles. The dimension of each tile is 914.4 m × 914.4 m. Original data acquisition was carried out by the Pictometry International's (Rochester, USA) using Optech's

Table 1
Summary statistics[†] of field-measured carbon density: mean, median, maximum, minimum and standard deviation.

Species group	Mean	Median	Std. deviation	Minimum	Maximum
Deciduous	121.63	110.03	58.93	26.54	298.46
Coniferous	66.77	62.20	33.15	21.17	165.89
Mixed	87.85	84.42	34.36	20.94	154.05

[†] The unit of all the statistics is t/ha.

ALTM Gemini 3100 LiDAR system (Optech Incorporated, Vaughan, Canada) with 1 mission on April 11th, 2012, 2 missions on April 12th, 2012, 1 mission on April 13th, 2012, and 2 missions on April 14th, 2012. Data were collected at a nominal point density of 1.0 point/m^2, with four returns from each pulse. Raw point clouds were generated using Applanix POSPac v4.4 (Applanix Corp., Richmond Hill, Canada) and the DashMap software package (Optech Incorporated, Vaughan, Canada). TerraMatch (Terrasolid Ltd., Helsinki, Finland) was used to measure and apply small adjustments to the system's orientation angles in order to ensure proper alignment of data between flight lines.

2.4. National Agriculture Imagery Program (NAIP) imagery

A multispectral NAIP (National Agriculture Imagery Program) mosaic, hereafter referred to as *NAIP image*, covering the study area was downloaded from the USDA Geospatial Data Gateway (http://datagateway.nrcs.usda.gov/). Original NAIP images were taken during the leaf-on season in 2012 at 1.0 m spatial resolution with four spectral bands (blue, range of wavelength: 400–580 nm; green, range of wavelength: 500–650 nm; red, range of wavelength: 590–675 nm; and near infrared, range of wavelength: 675–850 nm). The image was orthorectified with data quality inspected before it was delivered by the vendor (U.S. Department of Agriculture, 2014). GPS was further used to examine the geometric accuracy of the downloaded NAIP image, which revealed an average horizontal error of less than 3 m. Because carbon estimation was conducted at the spatial resolution of 20 m × 20 m (see details in Section 2.6), the geometric accuracy of the NAIP image met our needs.

2.5. Object-based neighborhood analysis

2.5.1. Object-based image classification

Geographic object-based image analysis (GEOBIA) provides an appropriate solution to capture and analyze meaningful ground objects while reducing high spectral variability in high-spatial resolution (i.e., typically higher than 5 m) imagery (Blaschke et al., 2014; Chen et al., 2012; Wulder, Hall, Coops, & Franklin, 2004). From the geography perspective, an object can be defined as a relatively homogenous area that differs from its surroundings. This term is often used to represent *patch* in landscape ecology. To calculate landscape metrics that quantify the characteristics of patches, a GEOBIA segmentation approach was firstly applied to extract objects. Specifically, we used eCognition Developer 8 (Trimble Navigation, Sunnyvale, California) to segment the four-band NAIP image with each band assigned the same weight. After a trial-and-error test, the spatial scale parameter (defining *mean object size*) of 30 was used to derive *image objects* aiming to capture high heterogeneity in the urban area (e.g., small tree clusters and individual houses). Here, image objects are clusters of neighboring pixels to represent meaningful ground objects. Identifying the class of each image object is important, as different land-cover and land-use (LCLU) types may affect forest carbon density in different ways. This process was accomplished by applying the classic supervised nearest neighbor classification algorithm to all the NAIP image objects using eCognition Developer 8. Besides the four spectral bands, spectral variation (i.e., standard deviation) of each spectral band within each image object was also computed and used in the classification. Six LCLU classes were finally generated including deciduous, coniferous, built-up, open space, water, and bare soil. Both training and reference samples (300 each) were randomly extracted from all the image objects. The LCLU types of these samples were identified through manual photo interpretation and field visits. A confusion matrix was generated with user's accuracy, producer's accuracy, overall accuracy, and kappa statistic calculated to evaluate the classification result (Congalton & Green, 1999).

2.5.2. Neighborhood selection

There are a total of 464 Neighborhood Profile Areas (NPA) in Mecklenburg County as defined by the 2012 Charlotte–Mecklenburg Quality of Life study (City of Charlotte and Mecklenburg County, 2014). These NPAs were developed using the 2010 Census Block Group geography, with each NPA representing one or more census block groups. Because the residential neighborhoods are the emphasis of this study, the classification results (Section 2.5.1) were used to assess the ratio of residential land use in each neighborhood. It was considered as a residential neighborhood when the neighborhood had at least 75% of the built-up land use. Within each selected neighborhood, the classified NAIP image was applied to calculate *percent built-up* (PBU) (built-up area divided by total neighborhood area) demonstrating residential density. Finally, we selected 100 residential neighborhoods that were almost equally divided into four categories to represent four types of residential densities: low, PBU ≤ 15%; medium-low, 15% < PBU ≤ 25%; medium-high, 25% < PBU ≤ 40%; and high, PBU > 40%. Because there is no official classification of residential neighborhoods based on residential density, the thresholds were chosen with the main purpose to distinguish major residential conditions (e.g., homes condensedly developed, or homes with big yards covered by trees). The neighborhood number, average size and description of each category are presented in Table 2. Four samples representing these neighborhoods are shown in Fig. 3.

2.6. Forest carbon estimation

2.6.1. Calculation of plot-level carbon density

LiDAR metrics were calculated from raw point clouds using FUSION, a widely-used free LiDAR processing package (McGaughey, 2014). Prior to the extraction of metrics, two steps were applied to

Table 2
Residential neighborhood categories (low, medium-low, medium-high and high density) with the selected number and average size of neighborhoods and their characteristics.

Category	Number	Average size (ha)	Characteristics
Low (PBU† ≤ 15%)	22	775	Forest dominated neighborhoods with patches of subdivisions. Areas of these neighborhoods tend to be larger than neighborhoods present in other categories
Medium-low (15% < PBU† ≤ 25%)	27	257	Suburban style development with reasonably large number of trees contained in the yards of homes. These neighborhoods also contain medium to large sized clumps of forested land
Medium-high (25% < PBU† ≤ 40%)	27	195	Condensed suburban style development with little to no trees contained in yards of homes. These neighborhoods contain small to medium disaggregated clumps of forested land
High (PBU† > 40%)	24	128	Mixed use neighborhoods containing residential areas and nearby business. They are typically developed in a very tight suburban style, including apartments and townhouses

† PBU: Percent built-up.

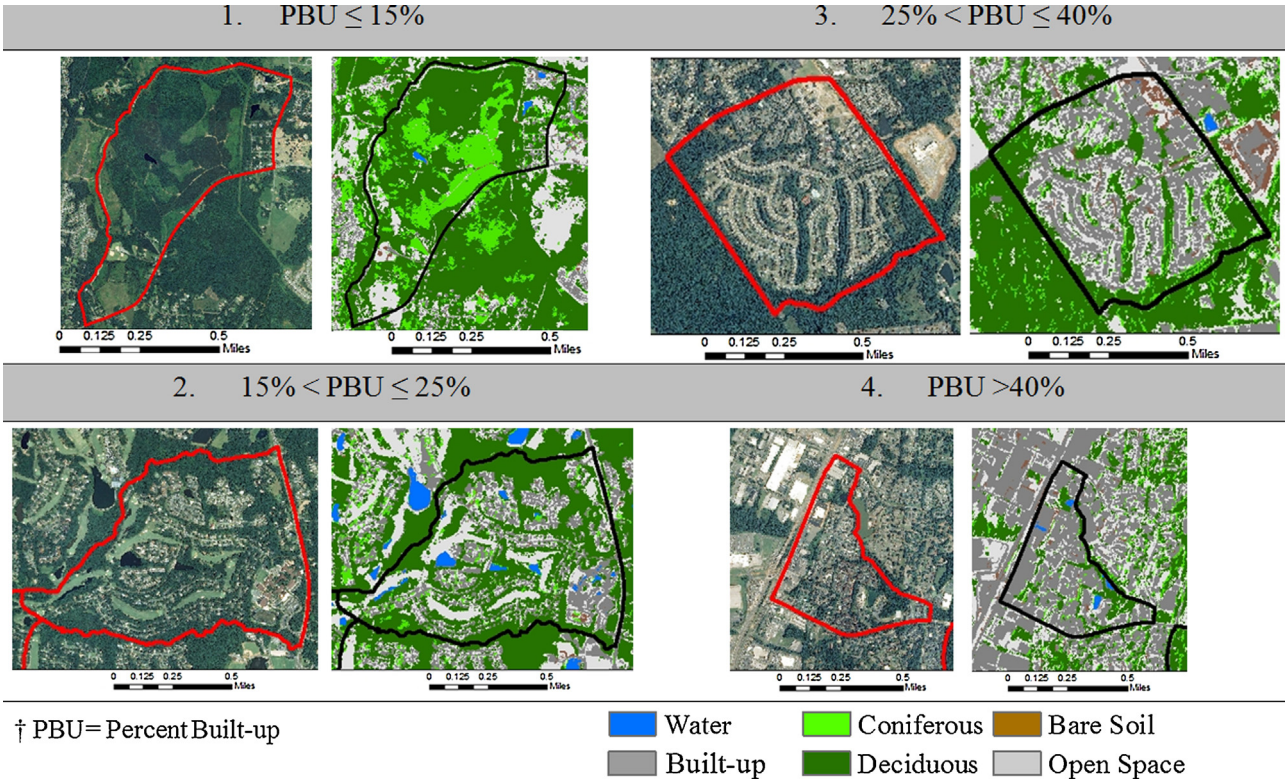

Fig. 3. Sample neighborhoods representing four types of residential densities of (1) low, (2) medium-low, (3) medium-high and (4) high. For each neighborhood, the red polygon shows the neighborhood boundary overlaid on the original NAIP true color composite, while the black polygon is the same boundary overlaid on the classified NAIP image. (For interpretation of the references to color in this figure legend, the reader is referred to the web version of this article.)

normalize LiDAR points and remove outliers. Specifically, the filter algorithm developed by Kraus and Pfeifer (1998) was used to distinguish ground points from non-ground points. Based on the ground points, we created a digital elevation model (DEM) for the entire study area, which was then applied to normalize LiDAR returns by removing the impact of surface topography. The outliers were eliminated using a height range from 2 m to 38 m that represents the actual growth condition of local trees. Consequently, a total of 25 metrics were extracted at the field plot level (Table 3). Similar lidar processing and metrics have been widely used in previous studies to estimate forest vertical structure in both the urban and natural environments (e.g., Shrestha & Wynne, 2012; Treitz et al., 2012).

Deciduous, coniferous and mixed plots contain different tree structures that should be modeled separately to account for variation in carbon storage (Chen & Hay, 2011; Popescu & Wynne, 2004). In this research, multiple regression models were developed to link LiDAR metrics (independent variables) with field-measured carbon density (dependent variable) at a 0.05 significance level. To overcome multicollinearity, variance inflation factor (VIF) was calculated for all the predictors. By following a common rule of thumb to avoid multicollinearity, the independent variables were selected where VIFs were smaller than 5 in the final models. As further suggested by several researchers (e.g., Hudak et al., 2006; Chen & Hay, 2011; Frazer, Magnussen, Wulder, & Niemann, 2011), nonlinear relationships between carbon density and forest structure often occur, and the transform of input variables using the natural logarithmic function and the Box–Cox transformation (a power transform) have the potential to improve the performance of LiDAR carbon modeling. The Box–Cox transformation, which is often used to achieve linearity in the model, was calculated in the form of an exponent containing the value λ (Eq. (1)). This value was derived by plotting the log likelihood against λ values, and finding the λ that was associated with the maximum log likelihood value for the model (Box & Cox, 1964). The logarithmic function is actually a special case of the Box–Cox transformation when zero is chosen for the λ parameter. Due to the limited number of field plots for each type of forest species, the leave-one-out cross validation was applied

Table 3
LiDAR metrics extracted from the raw point data and the corresponding abbreviations.

LiDAR metric	Abbreviation
Total return count	TRC
Minimum	Height.Min
Maximum	Height.Max
Mean	Height.Mean
Mode	Height.Mode
Standard deviation	Height.Stddev
Variance	Height.Var
Skewness	Height.Skew
Kurtosis	Height.Kurt
Height 1st percentile	Height.P01
Height 5th percentile	Height.P05
Height 10th percentile	Height.P10
Height 20th percentile	Height.P20
Height 25th percentile	Height.P25
Height 30th percentile	Height.P30
Height 40th percentile	Height.P40
Height 50th percentile	Height.P50
Height 60th percentile	Height.P60
Height 70th percentile	Height.P70
Height 75th percentile	Height.P75
Height 80th percentile	Height.P80
Height 90th percentile	Height.P90
Height 95th percentile	Height.P95
Height 99th percentile	Height.P99
Canopy relief ratio	CRR

to assess the model performance with both R^2 values and RMSEs (root-mean-squared errors) reported (Davis, 1987).

$$y^{(\lambda)} = \begin{cases} \dfrac{\left(y^{\lambda} - 1\right)}{\lambda}, & \lambda \neq 0 \\ \log(y), & \lambda = 0 \end{cases} \quad (1)$$

2.6.2. Calculation of landscape-level carbon density and forest value

The classified NAIP image was used as the base map for extracting deciduous, coniferous, and mixed forests for the entire city. Specifically, 0.04 ha square grids were overlaid to the area for the purpose of simulating field plots of the same size. Within individual grids, we followed the same criterion in field mensuration (Section 2.2) to determine within-grid forest species types by applying a threshold of 0.75. Specifically, if more than 75% of the grid pixels were classified as coniferous (or deciduous) trees, the grid was labeled as a coniferous (or deciduous) plot. If neither coniferous nor deciduous trees could dominate the grid area with more than 75% of coverage, and the area still had more than 75% of tree coverage, it was labeled as a mixed plot. LiDAR metrics (Table 3) were extracted for all the grids, which was followed by applying the three developed forest carbon models (Section 2.6.1) to map the wall-to-wall carbon density at the urban landscape level.

To estimate economic value associated with the carbon stored in Charlotte's urban forests, the total amount of carbon storage was multiplied by $78.5 (per tonne of carbon). The value of $78.5 was used on the basis of the social costs of carbon estimated in 2010, and has been recommended by the U.S. Government (2010) and Nowak et al. (2013). It should be noted that carbon markets are highly volatile, and the value of sequestered carbon depends on a range of social and regulatory factors (Zheng, Ducey, & Heath, 2013). Here, we did not intend to provide an accurate market price for the local trees that is in fact difficult to achieve. The main purpose was to deliver a preliminary monetary assessment of the urban forests growing in Charlotte–Mecklenburg County.

2.7. Statistical analysis

2.7.1. Calculation of landscape metrics

Landscape metrics, typically developed on the basis of information-theory measures and fractal geometry, have proven to be suitable for capturing the structures and patterns of a landscape since late 1980s (Herold et al., 2002; Riitters et al., 1995; Turner, 1989; Wu et al., 2003). While a variety of metrics are available for investigation, the challenge is twofold: first, many of the metrics are highly correlated; second, no single metric can represent all aspects of the complex urban patterns (Seto & Fragkias, 2005). In this study, we evaluated the impact of five aspects (i.e., area, shape, dispersion/interspersion, diversity, and connectivity) of spatial heterogeneity on forest carbon storage, by adopting six representative landscape metrics: percentage of landscape area (PLAND), mean patch size (MPS), edge density (ED), contagion index (CONTAG), Shannon's diversity index (SHDI), and patch cohesion index (COHESION) (Table 4; McGarigal et al., 2002). Specifically, PLAND was computed to represent the area percentage for each of the six LCLU classes. Different urban development patterns may change landscape composition in varying ways. For example, a high density residential area tends to contain a lower proportion of forest patches and a higher proportion of build-ups than a low density residential area. MPS was also calculated for each of the six LCLU classes, with the purpose to measure the extent of subdivision within neighborhoods. A smaller MPS often suggests a higher degree of fragmentation, although the interpretation should also take into account the size of neighborhood (McGarigal et al., 2002).

Table 4
Interpretation of the selected landscape metrics (McGarigal et al., 2002).

Landscape metric	Interpretation
Percentage of Landscape Area (PLAND)*	Value approaches 0 when the largest patch of the corresponding patch type becomes increasingly rare in the landscape. Equals 100 when the entire landscape consists of a single patch type
Mean Patch Size (MPS)*	A function of the number of patches in the class and total class area
Edge Density (ED) **	ED standardizes edge to a per unit area basis that facilitates comparisons of edge length among landscapes of varying size
Contagion Index (CONTAG)**	CONTAG measures the extent to which patch types are aggregated or clumped (i.e., dispersion); higher values of contagion may result from landscapes with a few large, contiguous patches, whereas lower values generally characterize landscapes with many small and dispersed patches
Shannon's diversity index (SHDI)**	SHDI equals 0 when the landscape contains only 1 patch (i.e., no diversity). SHDI increases as the number of different patch types (i.e., patch richness, PR) increases and/or the proportional distribution of area among patch types becomes more equitable
Patch cohesion index (COHESION)**	COHESION measures physical connectedness of the corresponding patch type. Value is sensitive to the aggregation of the focal class. As patch cohesion increases the patch type becomes more clumped or aggregated in distribution

* Class level metric, with six values computed for six classes in each neighborhood, including deciduous, coniferous, built-up, open space, water, and bare soil.
** Landscape level metric with one value calculated in each neighborhood.

Both PLAND and MPS are area-related landscape characteristics. ED is a measurement of patch shape complexity. Compared to the natural environments, anthropogenic features (e.g., buildings and parking lots) add higher patch diversity to the landscape, increasing the total length of edge, and thus edge density (Chen, Zhao, & Powers, 2014). CONTAG is an index that subsumes both dispersion and interspersion, and quantifies the extent to which patch types are clumped (McGarigal et al., 2002). Hence, landscapes with numerous small and dispersed patches are generally characterized by low CONTAG values (Herold, Couclelis, & Clarke, 2005). SHDI has been a popular index in ecology to measure species diversity in a given community (Magurran, 1988). Here, SHDI was calculated to measure the relative abundance of LCLU classes that were present in neighborhoods. By following Schumaker (1996), COHESION was computed to quantity the physical connectivity of patch types dispersing in landscapes. Generally, small COHESION values are often associated with highly subdivided landscapes (Yu & Ng, 2007). In this study, the widely-used Fragstats package was employed to calculate PLAND and MPS at the LCLU class level, and ED, CONTAG, SHDI and COHESION at the landscape level (McGarigal et al., 2002).

We note that the choice of 4 or 8-neighbor rule affects the delineation of patches, and thus the calculation of metrics. The 8-neighrbor rule was chosen in our tests, based on the consideration that both the cardinal and diagonal pixels/cells should be treated as adjacent neighbors, and such choice has proven effective in the landscape and/or forest literature (Linke, Franklin, Huettmann, & Stenhouse, 2005; Marceau & Moreno, 2008; Richardson & Moskal, 2011). We further compared the values of landscape metrics using these two rules, and found that the choice of rule (i) had no impact

on PLAND, ED, CONTAG, and SHDI, (ii) only slightly altered COHESION values by less than 0.03% for the four types of residential neighborhoods, and (iii) changed MPS values by less than 6% across the neighborhoods with *t*-test showing no significant difference ($p > 0.05$) between 4 and 8-neighbor MPS values.

2.7.2. Impact of neighborhood development patterns

Neighborhoods with various residential densities directly change how urban forests are fragmented, which may have different impacts on forest carbon storage. In this study, we first summarized and compared all the selected landscape metrics for the four types of residential neighborhoods of low, medium-low, medium-high and high density. *t*-Test was employed to assess whether different types of neighborhoods (i.e., urban development patterns) have resulted in significantly different landscape metric values. Then, carbon density was calculated within each neighborhood by dividing the total amount of forest carbon storage by the area of canopy cover. Spearman's correlation coefficients were calculated to evaluate the relationship between forest carbon density and the selected landscape metrics for the four types of neighborhoods and all the neighborhoods, respectively (Hollander & Wolfe, 1973). Because such relationships are potentially nonlinear, Spearman's correlation is suitable to assess whether two variables can be described using a monotonic function; while the commonly-used Pearson's correlation only measures the linear relationships between variables. Spearman's coefficient ranges from −1 to +1. If forest carbon density and the selected landscape metrics are monotonically related, Spearman's coefficient is close to 1, even if they are not linearly related. Spearman's coefficient is close to 0 when the data are roughly elliptically distributed.

3. Results

3.1. Object-based image classification

A total of six LCLU classes were generated using the object-based image classification, with an overall accuracy of 83.92%, and kappa statistic of 0.84. Among all the classes, forests occupied approximately 50% of the Charlotte region (deciduous: 44.65%; coniferous: 5.51%; Fig. 4). The user's and producer's accuracies for deciduous and coniferous trees were 82.57% and 86.54%, and 81.48% and 75.86%, respectively (Table 5). Particularly for deciduous trees, errors were partially introduced by misclassification between trees and open space. Besides forests, the other four classes accounted for 22.65% (built-up), 21.59% (open space), 3.46% (water), and 2.14% (bare soil) of the region, respectively (Fig. 4). The highest classification accuracy was achieved for water (user's accuracy: 100.00%; producer's accuracy: 96.00%; Table 5).

3.2. Plot-level carbon density models

Separate carbon density models were developed for the three forest types (i.e., deciduous, coniferous and mixed) using plot-level field measurements and LiDAR metrics (Table 6). Among them, the best performance was achieved by modeling coniferous trees ($R^2 = 0.86$ and RMSE = 11.84 t/ha). For the deciduous tree plots, the model explained 74% of the carbon variance (RMSE = 12.82 t/ha); while for the mixed tree plots, the model accounted for 56% of the carbon variance (RMSE = 13.56 t/ha). The results suggest that modeling carbon storage in deciduous trees is more difficult than that in coniferous trees. Similar findings were also reported by previous studies for the estimation of forest vertical structure and biomass (Boudreau et al., 2008; Popescu & Wynne, 2004). This could be explained by the fact that deciduous trees have irregular shaped canopy with high variation (Chen, Hay, Castilla, St-Onge, & Powers, 2011). Even for the same species, canopy shape and tree growth

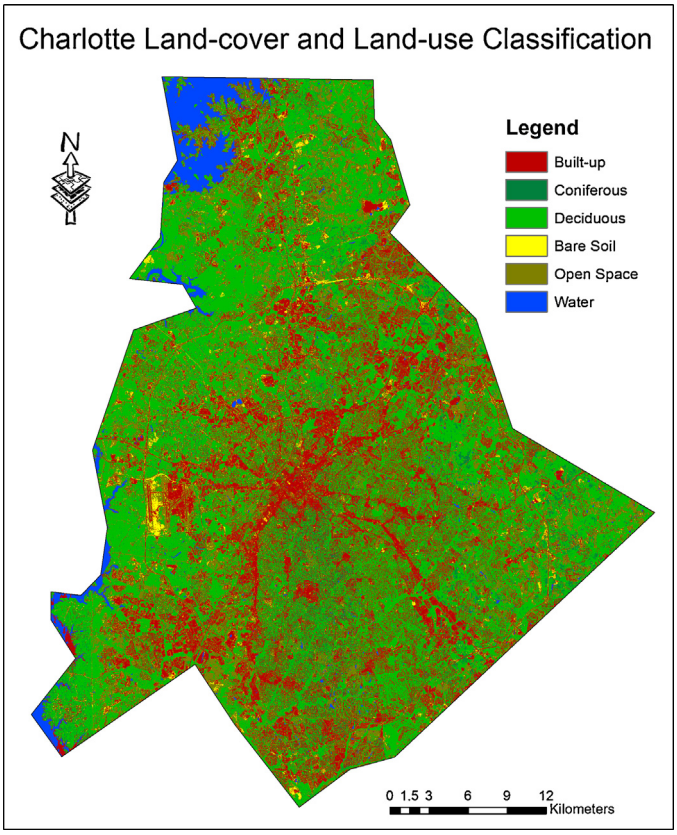

Fig. 4. Charlotte land-cover and land-use classification result using geographic object-based image analysis (GEOBIA).

are highly affected by a variety of microclimate and local environmental factors. In an urban setting, the impacts from these factors are non-stationary and contain high heterogeneity. For instance, anthropogenic disturbances may create large open spaces (e.g., a backyard) for trees to branch freely or influence tree crown size and shape with man-made features (e.g., trees adjacent to a building).

The final carbon density models developed for the three forest types had different forms after the assessment of natural logarithmic and Box–Cox transformations (Table 6). Specifically, simple linear regression best modelled the relationship between the carbon stored in coniferous trees and LiDAR metrics. For the deciduous plots, a Box–Cox power transformation was selected to transform the dependent variable of carbon density, and the natural logarithmic transform was applied to the independent variables of LiDAR metrics. The final form of the deciduous carbon model was chosen after a thorough evaluation of model accuracy using various combinations of transformation. In this model, if no transformation was used, the model only explained 20% of the variance related to carbon density, while the application of Box–Cox and natural logarithmic transformations led to a 53% increase (Table 6). For the mixed forest plots, we received the best carbon estimation result by using the natural logarithmic transformation on all the variables in the model. With no transformation applied, the model only accounted for 47% of the carbon variance compared to 56% with transformations (Table 6). We further noticed that a universal LiDAR model has proven sufficient in carbon estimation of natural forests with good performance (e.g., $R^2 = 0.80$, RMSE = 27.6 t/ha) regardless of forest types (Asner et al., 2012; Lefsky et al., 2002). However, the relationship between LiDAR metrics and forest carbon density in an urban environment tends to vary across tree types as evidenced by this study. Especially for the deciduous trees, they have irregular shaped canopies and the tree crowns are often

Table 5
Confusion matrix and kappa statistic of the geographic object-based image classification result.

User class	Reference class							
	Built-up	Coniferous	Deciduous	Bare soil	Open space	Water	Total	User's accuracy (%)
Built-up	52	0	5	8	2	1	68	76.47
Coniferous	2	22	3	0	0	0	27	81.48
Deciduous	0	7	90	1	11	0	109	82.57
Bare soil	0	0	0	20	0	0	20	100.00
Open Space	2	0	6	0	44	0	52	84.62
Water	0	0	0	0	0	24	24	100.00
Total	56	29	104	29	57	25	300	
Producer's accuracy (%)	92.86	75.86	86.54	68.97	77.19	96.00		

Overall accuracy = 83.92%; Kappa statistic = 0.84.

Table 6
The plot-level carbon density models, adjusted R^2 and RMSEs for the three forest types.

Species Group	Model	Adjusted R^2	RMSE (t/ha)
Deciduous	$Y^{-0.5} = (\ln(\text{abs}(Height.Skew)) \times (-0.01) + \ln(Height.P95) \times (-0.08) + \ln(Height.P05) \times (0.01) + \ln(TRC) \times (-0.01) + \ln(Height.Min) \times (-0.06) + 0.66$	0.74	12.82
Coniferous	$Y = Height.P05 \times (4.94) + TRC \times (0.01) + Height.Var \times (0.22) - 32.97$	0.86	11.84
Mixed	$\ln(Y) = \ln(Height.P01) \times (-0.11) + \ln(\text{abs}(Height.Skewness)) \times (-0.11) + \ln(Height.P40) \times (1.26) + 0.17$	0.56	13.56

Y = estimate of plot-level carbon density; *Height.Skew* = skewness; *TRC* = total return count; *Height.Min* = height minimum; *Height.Var* = height variance; *Height.P01* = Height 1st percentile; *Height.P05* = Height 5th percentile; *Height.P40* = Height 40th percentile; *Height.P95* = Height 95th percentile.

reformed as a result of inconsistent anthropogenic disturbances. Despite the high complexity, LiDAR remained a valuable tool in our forest carbon estimation when an appropriate variable transformation was applied. Fig. 5 shows the standard errors of carbon model estimates for (a) deciduous, (b) coniferous, and (c) mixed plots. All residuals appear to behave randomly suggesting that the selected models fit the data without apparent bias.

3.3. Landscape-level carbon density estimates

The average carbon density of the forested areas in the Charlotte–Mecklenburg County was estimated at 53.6 t/ha, with a total amount of 3.8 million tonnes. From the monetary value perspective, the carbon stored in urban trees was worth $298 million. The wall-to-wall carbon density map (Fig. 6) illustrates a general decrease of forest carbon storage from the county fringe to the center, corresponding to a spatial shift from low-density to high-density residential neighborhoods. This was further confirmed by the summarized carbon density statistics (i.e., mean, median, maximum, minimum and standard deviation) for the four types of neighborhoods (i.e., low, medium-low, medium-high and high density) as shown in Table 7. Specifically, the increase of built-up areas led to a constant decrease of forest carbon density from 61.86 t/ha (low-density residential) to 42.29 t/ha (high-density residential). It should also be noted that the variance of carbon estimates (i.e., standard deviation) increased as the percent built-up increased within the neighborhoods. The maximum carbon density in the high-density residential category was similar to that in the low-density category (73.46 versus 78.08 t/ha). This finding confirmed that forest ecosystems are highly influenced by various urban spatial patterns. Especially in a highly developed area, even if two neighborhoods have exactly the same percentage of canopy cover, carbon density is likely to be different under varying land development regulations.

3.4. Neighborhood development patterns

Pattern analysis indicates that the four types of residential neighborhoods changed urban landscapes in varying ways (Fig. 7). For example, deciduous trees that covered approximately 45% of the entire region showed a significant (t-test, $p < 0.05$) decrease of average patch size (i.e., MPS) from 0.53 ha to 0.14 ha, from low

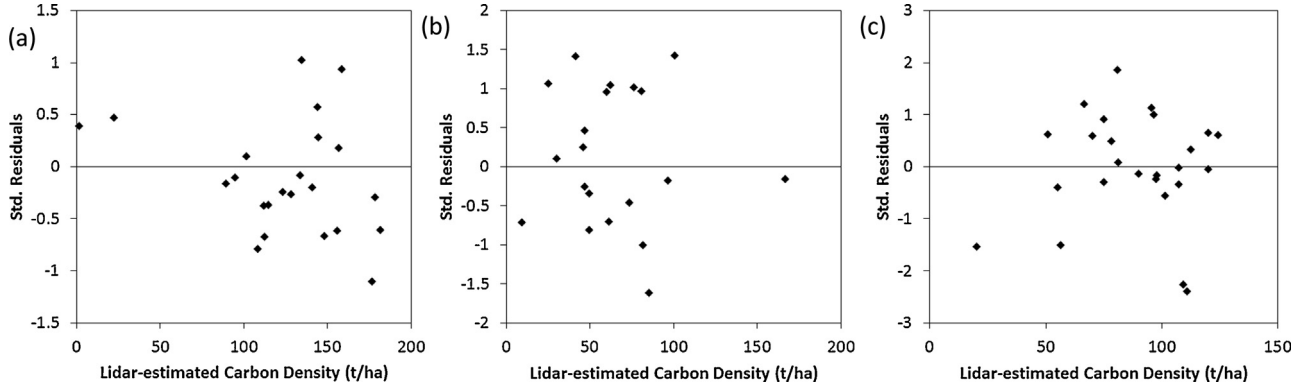

Fig. 5. Standardized residuals of carbon model estimates for (a) deciduous, (b) coniferous, and (c) mixed plots.

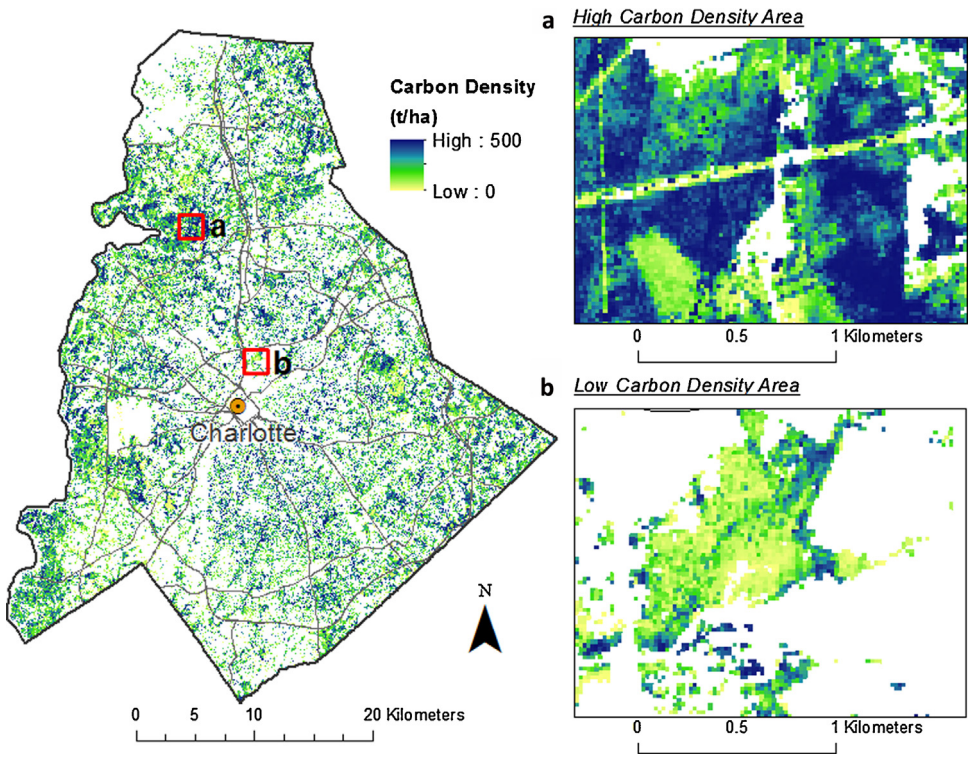

Fig. 6. A wall-to-wall carbon density map of Charlotte–Mecklenburg County, North Carolina. Insets (a) and (b) illustrate sampler high and low carbon density areas, respectively.

Table 7
Summary statistics[†] of carbon density for the four types of residential neighborhoods.

Category	Mean	Median	Std. deviation	Minimum	Maximum
Low (PBU[‡] ≤ 15%)	61.86	63.63	9.34	41.74	78.08
Medium-low (15% < PBU ≤ 25%)	58.22	58.54	9.86	41.94	76.61
Medium-high (25% < PBU ≤ 40%)	52.3	52.12	12.17	32.12	76.49
High (PBU > 40%)	42.29	41.16	17.83	13.06	73.46

[†] The unit of all the statistics is t/ha.
[‡] PBU: percent of built-up land.

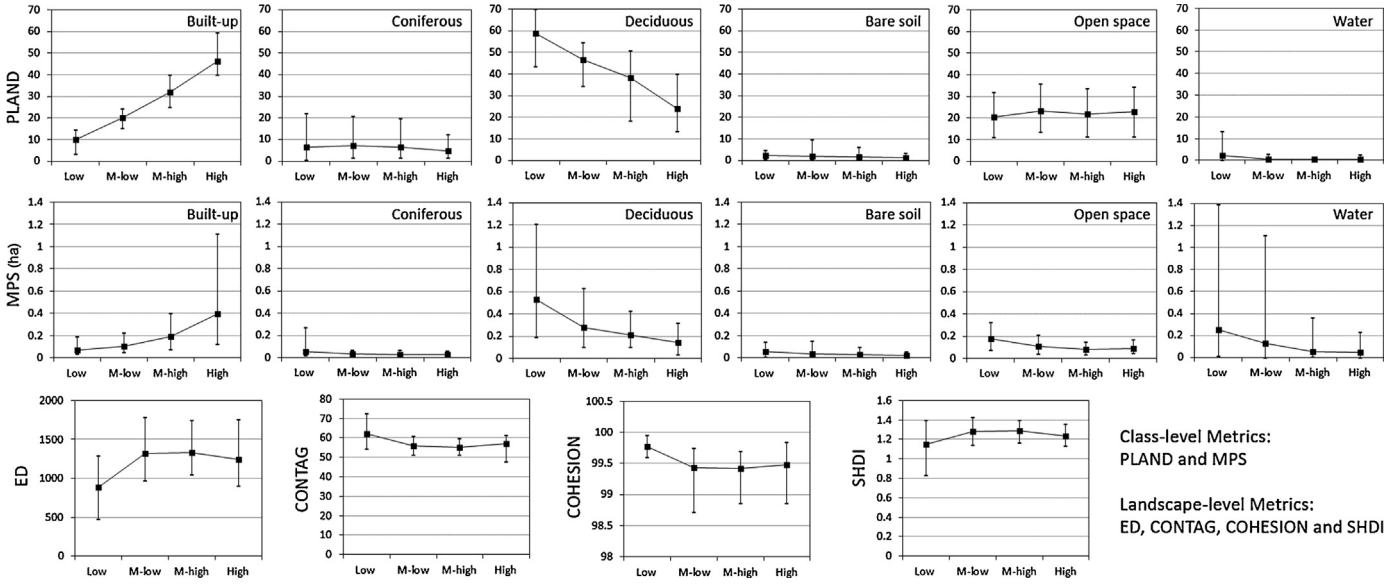

Fig. 7. Stock charts of the selected landscape metrics (i.e., PLAND: percentage of landscape area; MPS: mean patch size; ED: edge density; CONTAG: contagion index; SHDI: Shannon's diversity index; and COHESION: patch cohesion index) for four types of residential neighborhoods (Low: low density; M-low: medium-low density, M-high: medium-high, and High: high density). Maximum, minimum and average values are presented for each metric.

Table 8
Spearman's correlation coefficients between forest carbon density and the selected landscape metrics across low, medium-low, medium-high, and high density neighborhoods.

Landscape metric	Low density neighborhoods	Medium-low density neighborhoods	Medium-high density neighborhoods	High density neighborhoods	All neighborhoods
PLAND_C1	0.03 ns	0.06 ns	−0.37 ns	−0.01 ns	−0.46**
PLAND_C2	0.03 ns	0.12 ns	−0.01 ns	−0.10 ns	0.10 ns
PLAND_C3	−0.04 ns	0.44*	0.63**	0.67**	0.58**
PLAND_C4	0.01 ns	−0.22 ns	−0.06 ns	−0.09 ns	0.05 ns
PLAND_C5	0.21 ns	−0.63*	−0.62 ns	−0.56**	−0.42**
PLAND_C6	−0.06 ns	0.17 ns	0.08 ns	0.24 ns	0.16 ns
MPS_C1	−0.08 ns	0.07 ns	−0.48*	0.21 ns	−0.40**
MPS_C2	−0.20 ns	0.12 ns	0.02 ns	0.06 ns	0.23*
MPS_C3	−0.21 ns	0.45*	0.59**	0.81**	0.61**
MPS_C4	−0.10 ns	−0.14 ns	0.16 ns	0.19 ns	0.24**
MPS_C5	0.29 ns	−0.38 ns	−0.37 ns	−0.23 ns	0.04 ns
MPS_C6	0.14 ns	0.12 ns	0.01 ns	0.09 ns	0.22*
ED	0.25 ns	−0.23 ns	−0.21 ns	−0.59**	−0.33**
CONTAG	−0.13 ns	0.27 ns	0.26 ns	0.32 ns	0.25*
COHESION	0.11 ns	0.32 ns	−0.19 ns	0.22 ns	0.26**
SHDI	0.04 ns	−0.25 ns	−0.17 ns	−0.07 ns	−0.14 ns

Significance levels: * $p < 0.05$; ** $p < 0.01$.
ns: $p > 0.05$. PLAND: percentage of landscape area; MPS: mean patch size; ED: edge density; CONTAG: contagion index; SHDI: Shannon's diversity index; and COHESION: patch cohesion index. C1: built-up; C2: coniferous, C3: deciduous, C4: bare soil; C5: open space; and C6: water.

to high residential density neighborhoods. The corresponding average area percentage values (i.e., PLAND) significantly ($p < 0.05$) decreased from 58.82% to 24.03% as well. Conversely, MPS and PLAND for the built-up exhibited significant ($p < 0.05$) increase from 7.12 ha to 39.57 ha, and from 9.87% to 46.34%, respectively. This was expected because one of the major types of LCLU change in urbanized regions (including Charlotte) is the conversion from forests to build-ups (Herold et al., 2005; Seto & Fragkias, 2005). However, the sizes and percentages of coniferous patches remained relatively stable across the four types of neighborhoods. This is possible due to the protection activities implemented by local communities since coniferous trees only accounted for 5.51% of the entire region (Fig. 4).

As another major LCLU class occupying 21.59% of the area, open space showed an unexpected pattern, which was different from the patterns unveiled by both the forest and built-up classes (Fig. 7). Initially, we anticipated that open space should have smaller patch sizes in higher density neighborhoods. However, its MPS showed no significant change ($p > 0.05$) across medium-low, medium-high and high density neighborhoods. MPS only disclosed a significant ($p < 0.05$) decrease from low to medium-low density neighborhoods (from 0.18 ha to 0.11 ha). This may have reflected the past and current urban planning regulations enforced in the area. Similarly, bare soil showed no significant ($p > 0.05$) change of patch size and area percentage across the neighborhoods with varying residential densities (Fig. 7). This is due to the fact that bare soil in the region typically represented areas under new constructions (e.g., new houses or roads), and such activities have occurred with no bias to specific neighborhood types.

At the landscape level, Fig. 7 shows that low density neighborhoods have the lowest degree of patch shape complexity (ED = 880.25) and diversity (SHDI = 1.15), and the highest degree of aggregation (CONTAG = 61.97) and patch connectivity (COHESION = 99.78). This makes sense because these neighborhoods were covered by large portions of forests, subject to a low level of anthropogenic disturbances. Similar findings were also reported by other urban researchers (Herold et al., 2005; Ren et al., 2013; Seto & Fragkias, 2005). With the increase of built-up coverage (i.e., for medium-low, and medium-high density neighborhoods), ED and SHDI significantly ($p < 0.05$) increased with CONTAG and COHESION decreased (Fig. 7). However, Fig. 7 further demonstrates that the four metrics start to reveal an opposite trend, when the neighborhoods are comprised of more than 40% of build-ups (i.e., high density neighborhoods). This can be explained by the fact that urban build-ups gradually replaced forests as the major LCLU class in the neighborhoods. Even though, the development patterns extracted from the high density neighborhoods were found to be more similar to those of medium-low and medium-high density neighborhoods, rather than the low density neighborhoods.

3.5. Relationships between neighborhood pattern and carbon density

Spearman's correlation (ρ) was calculated to identify the monotonic relationship between forest carbon density and each of the selected landscape metrics with results presented in Table 8. Surprisingly, none of the landscape metrics unveiled a significant correlation with carbon density in the low density neighborhoods. Since most of these neighborhoods were dominated by forests, tree growth may have been highly correlated with local species types and environmental factors, such as topography and precipitation. With urban landscapes increasingly affected by human activities, the role that the selected landscape metrics played in determining carbon density became gradually apparent. For the high density neighborhoods, the metrics of deciduous patch size (MPS_C3) and area percentage (PLAND_C3) demonstrated strong and positive correlations with carbon density ($\rho_{MPS\_C3} = 0.81$; $\rho_{PLAND\_C3} = 0.67$) at the significance level of 0.01 (Table 8). Meanwhile, the area percentage of open space and edge complexity were negatively correlated with carbon density ($\rho_{PLAND\_C5} = -0.56$; $\rho_{ED} = -0.59$).

4. Discussions

4.1. Uncertainties in image classification

In the study area, most of the open space was equivalent to grass space (e.g., lawn). The spectral reflectance from grass and broadleaf trees were similar in both the visible and near infrared bands that together comprised the NAIP image. In fact, we found that such misclassification was often biased to open space, where an open space object with high spectral variation was likely to be misclassified as deciduous trees. Another source of error was misclassification caused by the 3D geometry of terrestrial surfaces. In high-resolution optical imagery (i.e., 1 m NAIP in our case), detailed spatial information can be easily observed. However, one side effect is that forest canopies and anthropogenic features often cast shade on the neighboring surfaces that have lower elevations. The mixed spectral information from these surfaces could possibly

reduce classification accuracy. Although the use of GEOBIA has proven effective to mitigate such effect (Blaschke et al., 2014), misclassification of some boundary objects between tree patches and build-ups or open space remained. This was also the major source of error for extracting the built-up class (Table 5).

Due to specular reflection, the reflected radiation from water bodies is normally within a narrow cone in space. In most cases, remote sensors are only able to capture a small portion of such energy, resulting in low spectral reflectance from lakes, rivers or ponds. Hence, water bodies were easily distinguished from the other LCLU features. However, we note that the reflectance from water is also relevant to the concentration of suspended sediments, which could increase uncertainties in classification (Han, 1997). It was further discovered that some bare soil objects were misclassified as build-ups. Most of the bare soil areas were the sites experiencing new constructions (e.g., from forest to residential), where the surfaces (e.g., temporary unpaved roads) showed the similar high reflectance as some of the impervious surfaces.

4.2. Carbon density estimation

The historical carbon storage in Charlotte forests was not well documented, hence our result was evaluated through an inter-city comparison, and was similar to the carbon density estimate in the city of Atlanta (66.3 t/ha) (Nowak et al., 2013). As southeastern U.S. cities, both regions are geographically close, and share similar types of dominant temperate broadleaf forests. However, the comparison also indicates that Charlotte trees per hectare have stored less carbon than the trees growing in Atlanta. This may be partially explained by the application of different approaches in carbon estimation (i.e., remote sensing versus field mensuration). For the Atlanta case, limited number of field plots was used, which can provide accurate carbon estimates at the plots, but may have introduced a sampling error. Our result was created by summarizing the LiDAR-measured wall-to-wall carbon estimates across the entire forested areas. Trees that are subject to various degrees of anthropogenic disturbances are likely to lock up carbon at different levels. For example, Liu and Li (2012) reported that a highly fragmented road forest stores much less carbon than a landscape and relaxation forest (13.17 versus 33.65 t/ha) in an urban setting. Remote sensing has the capacity to account for such high level of fragmentation; however, we recognize the errors and uncertainties in upscaling field carbon measurements using LiDAR models.

4.3. Impact of urban development on forest carbon density

The derived Spearman's correlation coefficients in Table 8 demonstrate that: (i) single landscape metrics tend to have difficulties to consistently contribute to a significant carbon-pattern relationship in the neighborhoods of varying residential density types. However, (ii) patch area characteristics (e.g., area percentage) of the dominant forest types (i.e., deciduous trees in our study) have a high potential to influence carbon density for most of the neighborhoods that are subject to a relatively high level of anthropogenic disturbances. (iii) Residential neighborhoods, which have experienced a higher degree of development intensity (i.e., higher built-up coverage), are possibly affected by a larger number of spatial pattern metrics. Consequently, forest carbon density may exhibit higher variations across these neighborhoods. This is evident in our study (Table 7), where the carbon density standard deviation values were found to progressively increase from 9.34 t/ha (low density residential) to 17.83 t/ha (high density residential).

Analyses of landscape patterns in urban environments often treat cities as homogenous (e.g., Herold et al., 2005; Ren et al., 2013). However, Grove et al. (2006) and Zhao et al. (2010) reported that the differences in tree management practices or land-use types can exert high impacts on forest carbon storage across neighborhoods. So, should the assessment of the pattern-carbon relationship be conducted at the neighborhood level or the city level? What are the differences? To address the questions, our study further quantified the relationship between carbon density and the selected landscape metrics for all the neighborhoods combined together (i.e., without distinguishing neighborhoods of varying density types). Compared to our findings extracted from the individual neighborhood types, a larger number of landscape metrics (i.e., 11 out of the total 16) were found to be significantly correlated with carbon density at the city level (Table 8). This suggests that distinct policies should be developed to recognize the scale-induced variation in supporting city- and neighborhood-level forest management and sustainability.

5. Conclusions

The amount carbon stored by urban forests is highly influenced by city development patterns. Evaluating their relationship can inform on urban sustainability planning and design. However, this practice is often impeded due to the lack of large-area and spatially explicit carbon estimates. In this study, LiDAR, aerial photography and field mensuration were integrated to map forest carbon density over the 1415 km^2 Charlotte Metropolitan Area in the United States, which was followed by a statistical analysis of the relationship between landscape metrics and forest carbon density in four types of residential neighborhoods with built-up density from low, medium-low, medium-high, to high. Our results demonstrate a total amount of 3.8 million tonnes carbon ($298 million value) in the Charlotte metropolitan region, with an average carbon density of 53.6 t/ha. The selected landscape metrics that significantly influenced tree carbon storage varied across different types of neighborhoods, although the area percentage of deciduous trees (the local dominant forest type) had a significant and positive correlation with carbon density across most of the neighborhoods. It was further discovered that residential neighborhoods with higher built-up coverage were more likely to be affected by a larger number of spatial pattern metrics, and their carbon density values unveiled a higher degree of variation. This suggests that it is possible to dramatically enhance the ability of forest carbon storage at the landscape level by designing proper policies to inform on urban spatial development at the neighborhood level. With high-spatial resolution remote sensing datasets becoming gradually available in more regions, the framework developed for the Charlotte area can also be applied to studying the relationship between forest carbon density and neighborhood development patterns in many other cities. However, it should be noted that the presented framework needs to be well calibrated and validated before the conclusions can be made to support urban sustainability, because model errors may propagate through the calculations within major processing steps, including field carbon estimation, LCLU classification, remote sensing carbon modeling, neighborhood delineation, and landscape metric extraction.

Acknowledgements

We gratefully acknowledge the financial support from North Carolina Space Grant, the University of North Carolina at Charlotte Faculty Research Grant, and the College of Liberal Arts and Sciences Seed Grant. We thank the Charlotte–Mecklenburg County Government for providing the LiDAR data, Dr. Ross Meentemeyer for supporting field data acquisition, and the insightful comments from the editor and anonymous reviewers.

References

Asner, G. P., Mascaro, J., Muller-Landau, H., Vieilledent, G., Vaudry, R., Rasamoelina, M., et al. (2012). A universal airborne LiDAR approach for tropical forest carbon mapping. *Oecologia*, *168*(4), 1147–1160. http://dx.doi.org/10.1007/s00442-011-2165-z

Blaschke, T., Hay, G. J., Kelly, M., Lang, S., Hofmann, P., Addink, E., et al. (2014). Geographic object-based image analysis–towards a new paradigm. *ISPRS Journal of Photogrammetry and Remote Sensing*, *87*, 180–191. http://dx.doi.org/10.1016/j.isprsjprs.2013.09.014

Boudreau, J., Nelson, R., Margolis, H., Beaudoin, A., Guindon, L., & Kimes, D. (2008). Regional aboveground forest biomass using airborne and spaceborne LiDAR in Québec. *Remote Sensing of Environment*, *112*(10), 3876–3890. http://dx.doi.org/10.1016/j.rse.2008.06.003

Box, G., & Cox, D. R. (1964). An analysis of transformations. *Journal of the Royal Statistical Society*, *26*(2), 211–252.

Cairns, M. A., Brown, S., Helmer, E. H., & Baumgardner, G. A. (1997). Root biomass allocation in the world's upland forests. *Oecologia*, *111*, 1L 11.

Congalton, R. G., & Green, K. (1999). *Assessing the accuracy of remotely sensed data: Principles and practices*. Boca Raton, FL: CRC, Press.

Chen, G., & Hay, G. (2011). An airborne LiDAR sampling strategy to model forest canopy height from Quickbird imagery and GEOBIA. *Remote Sensing of Environment*, *115*(6), 1532–1542. http://dx.doi.org/10.1016/j.rse.2011.02.012

Chen, G., Hay, G. J., Castilla, G., St-Onge, B., & Powers, R. (2011). A multiscale geographic object-based image analysis to estimate lidar-measured forest canopy height using Quickbird imagery. *International Journal of Geographical Information Science*, *25*(6), 877–893. http://dx.doi.org/10.1080/13658816.2010.496729

Chen, G., Wulder, M. A., White, J. C., Hilker, T., & Coops, N. C. (2012). LiDAR calibration and validation for geometric-optical modeling with Landsat imagery. *Remote Sensing of Environment*, *124*, 384–393. http://dx.doi.org/10.1016/j.rse.2012.05.026

Chen, G., Zhao, K., & Powers, R. (2014). Assessment of the image misregistration effects on object-based change detection. *ISPRS Journal of Photogrammetry and Remote Sensing*, *87*, 19–27. http://dx.doi.org/10.1016/j.isprsjprs.2013.10.007

City of Charlotte and Mecklenburg County. (2014). *Quality of life dashboard*. City of Charlotte and Mecklenburg County., <http://maps.co.mecklenburg.nc.us/qoldashboard> (last accessed October 15, 2014).

Clark, J. R., Matheny, N. P., Cross, G., & Wake, V. (1997). A model of urban forest sustainability. *Journal of Arboriculture*, *23*(1), 17–30.

Davis, B. M. (1987). Uses and abuses of cross-validation in geostatistics. *Mathematical Geology*, *19*, 241–248.

Escobedo, F. J., Adams, D. C., & Timilsina, N. (in press). Urban forest structure effects on property value. *Ecosystem Services*, 1–9. doi:10.1016/j.ecoser.2014.05.002.

Frazer, G. W., Magnussen, S., Wulder, M. A., & Niemann, K. O. (2011). Simulated impact of sample plot size and co-registration error on the accuracy and uncertainty of LiDAR-derived estimates of forest stand biomass. *Remote Sensing of Environment*, *115*(2), 636–649. http://dx.doi.org/10.1016/j.rse.2010.10.008

Grove, J. M., Cadenasso, M. L., Burch, W. R., Jr., Pickett, S. T., Schwarz, K., O'Neil-Dunne, J., et al. (2006). Data and methods comparing social structure and vegetation structure of urban neighborhoods in Baltimore, Maryland. *Society and Natural Resources*, *19*, 117–136.

Han, L. (1997). Spectral reflectance with varying suspended sediment concentrations in clear and algae-laden waters. *Photogrammetric Engineering & Remote Sensing*, *63*, 701–705.

Heath, L. S., Smith, J. E., Skog, K. E., Nowak, D. J., & Woodall, C. W. (2011). Managed forest carbon estimates for the US greenhouse gas inventory 1990–2008. *Journal of Forestry*, *109*(3), 167–173.

Herold, M., Couclelis, H., & Clarke, K. C. (2005). The role of spatial metrics in the analysis and modeling of urban land use change. *Computers, Environment and Urban Systems*, *29*, 369–399. http://dx.doi.org/10.1016/j.compenvurbsys.2003.12.001

Herold, M., Scepan, J., & Clarke, K. C. (2002). The use of remote sensing and landscape metrics to describe structures and changes in urban land uses. *Environment and Planning A*, *34*(8), 1443–1458. http://dx.doi.org/10.1068/a3496

Hollander, M., & Wolfe, D. A. (1973). *Nonparametric statistical methods*. New York, NY: Wiley.

Hudak, A. T., Crookston, N. L., Evans, J. S., Falkowski, M. J., Smith, A. M. S., Gessler, P. E., et al. (2006). Regression modeling and mapping of coniferous forest basal area and tree density from discrete-return lidar and multispectral satellite data. *Canadian Journal of Remote Sensing*, *32*(2), 126–138. http://dx.doi.org/10.5589/m06-007

Hudak, A. T., Strand, E. K., Vierling, L. A., Byrne, J. C., Eitel, J. U. H., Martinuzzi, S., et al. (2012). Quantifying aboveground forest carbon pools and fluxes from repeat LiDAR surveys. *Remote Sensing of Environment*, *123*, 25–40. http://dx.doi.org/10.1016/j.rse.2012.02.023

Jenkins, J. C., Chojnacky, D. C., Heath, L. S., & Birdsey, R. A. (2003). National-scale biomass estimators for United States tree species. *Forest Science*, *49*(1), 12–35.

Kraus, K., & Pfeifer, N. (1998). Determination of terrain models in wooded areas with airborne laser scanner data. *ISPRS Journal of Photogrammetry and Remote Sensing*, *53*(4), 193–203. http://dx.doi.org/10.1016/S0924-2716(98)00009-4

Lefsky, M. A., Warren, B., Cohen Hardings, D. J., Parker, G. G., Ackery, S. A., & Gower, S. T. (2002). Lidar remote sensing of above-ground biomass in three biomes. *Global Ecology and Biogeography*, *11*, 393–399.

Lieth, H. (1975). Modeling the primary productivity of the world. In H. Lieth, & R. H. Whittaker (Eds.), *Primary productivity of the biosphere* (pp. 237–263). Berlin: Springer-Verlag.

Linke, J., Franklin, S. E., Huettmann, F., & Stenhouse, G. B. (2005). Seismic cutlines, changing landscape metrics and grizzly bear landscape use in Alberta. *Landscape Ecology*, *20*(7), 811–826. http://dx.doi.org/10.1007/s10980-005-0066-4

Liu, C., & Li, X. (2012). Carbon storage and sequestration by urban forests in Shenyang, China. *Urban Forestry & Urban Greening*, *11*(2), 121–128. http://dx.doi.org/10.1016/j.ufug.2011.03.002

Lu, D. (2005). Aboveground biomass estimation using Landsat TM data in the Brazilian Amazon. *International Journal of Remote Sensing*, *26*(12), 2509–2525. http://dx.doi.org/10.1080/01431160500142145

Magurran, A. E. (1988). *Ecological diversity and its measurement*. Princeton, NJ: Princeton University Press.

Marceau, D. J., & Moreno, N. (2008). An object-based cellular automata to mitigate scale dependency. In T. Blaschke, S. Lang, & G. J. Hay (Eds.), *Object-based image analysis* (pp. 43–73). Berlin - Heidelberg: Springer-Verlag.

McGarigal, K., Cushman, S. A., Neel, M. C., & Ene, E. (2002). *FRAGSTATS: Spatial pattern analysis program for categorical maps*. Amherst, MA: University of Massachusetts.

McGaughey, R. J. (2014). *FUSION/LDV: Software for LIDAR data analysis and visualization*. Available online <http://forsys.cfr.washington.edu/fusion/fusionlatest.html> (last accessed October 15, 2014).

McPherson, E. G. (1998). Atmospheric carbon dioxide reduction by Sacramento's urban forest. *Journal of Arboriculture*, *24*(4), 215–223.

McPherson, E. G., Xiao, Q., & Aguaron, E. (2013). A new approach to quantify and map carbon stored, sequestered and emissions avoided by urban forests. *Landscape and Urban Planning*, *120*, 70–84. http://dx.doi.org/10.1016/j.landurbplan.2013.08.005

Myneni, R. B., Dong, J., Tucker, C. J., Kaufmann, R. K., Kauppi, P. E., Liski, J., et al. (2001). A large carbon sink in the woody biomass of Northern forests. *Proceedings of the National Academy of Sciences of the United States of America*, *98*(26), 14784–14789. http://dx.doi.org/10.1073/pnas.261555198

Nowak, D. J., Crane, D. E., Stevens, J. C., Hoehn, R. E., & Walton, J. T. (2008). A ground-based method of assessing urban forest structure and ecosystem services. *Arboriculture & Urban Forestry*, *34*(6), 347–358.

Nowak, D. J., Greenfield, E. J., Hoehn, R. E., & Lapoint, E. (2013). Carbon storage and sequestration by trees in urban and community areas of the United States. *Environmental Pollution*, *178*, 229–236. http://dx.doi.org/10.1016/j.envpol.2013.03.019

Plexida, S. G., Sfougaris, A. I., Ispikoudis, I. P., & Papanastasis, V. P. (2014). Selecting landscape metrics as indicators of spatial heterogeneity—A comparison among Greek landscapes. *International Journal of Applied Earth Observation and Geoinformation*, *26*, 26–35. http://dx.doi.org/10.1016/j.jag.2013.05.001

Popescu, S. C., & Wynne, R. H. (2004). Seeing the trees in the forest: Using lidar and multispectral data fusion with local filtering and variable window size for estimating tree height. *Photogrammetric Engineering & Remote Sensing*, *70*(5), 589–604.

Poudyal, N. C., Siry, J., & Bowker, J. M. (2011). Urban forests and carbon markets: Buyers' perspectives. *Journal of Forestry*, *109*(7), 378–385.

Ren, Y., Wei, X., Wang, D., et al. (2013). Linking landscape patterns with ecological functions: A case study examining the interaction between landscape heterogeneity and carbon stock of urban forests in Xiamen, China. *Forest Ecology and Management*, *293*, 122–131. http://dx.doi.org/10.1016/j.foreco.2012.12.043

Richardson, J. J., & Moskal, L. M. (2011). Strengths and limitations of assessing forest density and spatial configuration with aerial LiDAR. *Remote Sensing of Environment*, *115*(10), 2640–2651. http://dx.doi.org/10.1016/j.rse.2011.05.020

Riitters, K. H., Neill, R. V. O., Hunsaker, C. T., Wickham, J. D., Yankee, D. H., Timmins, S. P., et al. (1995). A factor analysis of landscape pattern and structure metrics. *Landscape Ecology*, *10*(1), 23–39.

Schmitt-Harsh, M., Mincey, S. K., Patterson, M., Fischer, B. C., & Evans, T. P. (2013). Private residential urban forest structure and carbon storage in a moderate-sized urban area in the Midwest, United States. *Urban Forestry & Urban Greening*, *12*(4), 454–463. http://dx.doi.org/10.1016/j.ufug.2013.07.007

Schumaker, N. H. (1996). Using landscape indices to predict habitat connectivity. *Ecology*, *77*, 1210–1225. http://dx.doi.org/10.2307/2265590

Seto, K. C., Güneralp, B., & Hutyra, L. R. (2012). Global forecasts of urban expansion to 2030 and direct impacts on biodiversity and carbon pools. *Proceedings of the National Academy of Sciences of the United States of America*, http://dx.doi.org/10.1073/pnas.1211658109

Seto, K. C., & Fragkias, M. (2005). Quantifying spatiotemporal patterns of urban land-use change in four cities of China with time series landscape metrics. *Landscape Ecology*, *20*(7), 871–888. http://dx.doi.org/10.1007/s10980-005-5238-8

Shrestha, R., & Wynne, R. H. (2012). Estimating biophysical parameters of individual trees in an urban environment using small footprint discrete-return imaging LiDAR. *Remote Sensing*, *4*, 484–508.

Singh, K. K., Vogler, J. B., Shoemaker, D. A., & Meentemeyer, R. K. (2012). LiDAR-Landsat data fusion for large-area assessment of urban land cover: Balancing spatial resolution, data volume and mapping accuracy. *ISPRS Journal of Photogrammetry and Remote Sensing*, *74*, 110–121. http://dx.doi.org/10.1016/j.isprsjprs.2012.09.009

Strohbach, M. W., & Haase, D. (2012). Above-ground carbon storage by urban trees in Leipzig, Germany: Analysis of patterns in a European city. *Landscape and Urban Planning*, *104*(1), 95–104. http://dx.doi.org/10.1016/j.landurbplan.2011.10.001

Termorshuizen, J. W., & Opdam, P. (2009). Landscape services as a bridge between landscape ecology and sustainable development. *Landscape Ecology*, *24*, 1037–1052.

Treitz, P., Lim, K., Woods, M., Pitt, D., Nesbitt, D., & Etheridge, D. (2012). LiDAR sampling density for forest resource inventories in Ontario, Canada. *Remote Sensing*, *4*(4), 830–848. http://dx.doi.org/10.3390/rs4040830

Turner, M. G. (1989). Landscape ecology: The effect of pattern on process. *Annual Review of Ecology, Evolution, and Systematics*, *20*, 171–197.

U.S. Government. (2010). *Technical support document: Social cost of carbon for regulatory impact analysis under executive order 12866*. U.S. Government., <http://www.epa.gov/oms/climate/regulations/scc-tsd.pdf> (last accessed October 15, 2014).

U.S. Census Bureau. (2013). *Annual estimates of the resident population*. U.S. Census Bureau., <http://www.census.gov/newsroom/releases/pdf/pep_2013_pepannres.pdf> (last accessed October 15, 2014).

U.S. Department of Agriculture. (2014). *Imagery programs: National Agriculture Imagery Program (NAIP)*. U.S. Department of Agriculture. <https://www.fsa.usda.gov/FSA/apfoapp?area=home&subject=prog&topic=nai> (last accessed October 15, 2014).

Yu, X. J., & Ng, C. N. (2007). Spatial and temporal dynamics of urban sprawl along two urban–rural transects: A case study of Guangzhou, China. *Landscape and Urban Planning*, *79*(1), 96–109. http://dx.doi.org/10.1016/j.landurbplan.2006.03.008

Wu, J., Shen, W., Sun, W., & Tueller, P. T. (2003). Empirical patterns of the effects of changing scale on landscape metrics. *Landscape Ecology*, *17*, 761–782.

Wulder, M. A., Hall, R. J., Coops, N. C., & Franklin, S. E. (2004). High spatial resolution remotely sensed data for ecosystem characterization. *BioScience*, *54*(6), 511–521. http://dx.doi.org/10.1641/0006-3568(2004)054[0511:HSRRSD]2.0.CO;2

Xiang, W. N. (2014). Doing real and permanent good in landscape and urban planning: Ecological wisdom for urban sustainability. *Landscape and Urban Planning*, *121*, 65–69. http://dx.doi.org/10.1016/j.landurbplan.2013.09.008

Zhao, M., Kong, Z. H., Escobedo, F. J., & Gao, J. (2010). Impacts of urban forests on offsetting carbon emissions from industrial energy use in Hangzhou, China. *Journal of Environmental Management*, *91*(4), 807–813. http://dx.doi.org/10.1016/j.jenvman.2009.10.010

Zheng, D., Ducey, M. J., & Heath, L. S. (2013). Assessing net carbon sequestration on urban and community forests of northern New England, USA. *Urban Forestry & Urban Greening*, *12*(1), 61–68. http://dx.doi.org/10.1016/j.ufug.2012.10.003